

Mass Renormalization in Transition Metal Dichalcogenides

T. Stroucken,¹ J. Neuhaus,¹ and S. W. Koch¹

¹*Department of Physics and Material Sciences Center,
Philipps University Marburg, Renthof 5, D-35032 Marburg, Germany*

(Dated: June 5, 2020)

It is shown that the three-fold rotational symmetry in transition metal dichalcogenides leads to a Coulomb induced renormalization of the effective electron and hole masses near the K -points of the Brillouin zone. The magnitude of the renormalization depends on the dielectric configuration. The effective exciton mass $m = 0.4m_0$ of a freely suspended MoS₂ monolayer changes to $m = 0.35m_0$ with hBN encapsulation. The mass renormalization increases the excitonic binding energy and reduces the exciton diamagnetic shift and cyclotron frequency. Detailed comparisons with high field measurements of the excitonic diamagnetic shift show excellent agreement.

With the ability to create them as monolayers, van der Waals bonded layers have emerged as a new material class, including graphene and transition metal dichalcogenides (TMDCs). In particular, TMDC monolayers have attracted considerable attention, partly because of their extraordinary strong light-matter interaction and excitonic effects, but also because of their potential application in valleytronic devices.

Common to TMDCs and other layered van der Waals materials is the arrangement of the atoms within the layers into a honeycomb lattice, with the atoms located at the corners of the hexagon. In reciprocal space, the first Brillouin zone also has honeycomb geometry with direct band gaps occurring at the six corners of the hexagon. Since neighboring K and K' valleys are related by the parity or time reversal transformation, these are addressed with oppositely circularly polarized light. This fascinating feature has led to fascinating new physics, in particular the novel concept of valleytronics[1–6].

Whereas the valley dependent optical selection rules are correctly predicted by density functional theory (DFT), the optical selection rules and the coupled spin-valley dynamics has been explained in a very elegant and intuitive manner by assigning relativistic quasi-particles with a pseudo-spin to the K and K' valleys. Since its proposal in the original work [1], the so called massive Dirac-Fermion model (MDF) Hamiltonian has been very successfully applied to describe many of the near K point electronic and optical TMDC properties [7–21]. [13] However, as we show in this Letter, the MDF Hamiltonian does not display the full three-fold rotational symmetry of the lattice, nor does it properly account for the change of orbital angular momentum of the basis functions upon absorption. We therefore propose a modified Hamiltonian (mMDF Hamiltonian) that incorporates the three-fold rotational symmetry. With this mMDF Hamiltonian, we obtain a Coulomb induced renormalization of the effective electron and hole masses near the K -point that increases the excitonic binding energy and reduces the exciton diamagnetic shift.

In its original form, the MDF Hamiltonian is given by

$$H_0 = \sum_{\tau\mathbf{sk}} \Psi_{\tau\mathbf{sk}}^\dagger \begin{pmatrix} \frac{\Delta_{s\tau}}{2} & \tau\hbar v_F k e^{-i\tau\theta_{\mathbf{k}}} \\ \tau\hbar v_F k e^{i\tau\theta_{\mathbf{k}}} & -\frac{\Delta_{s\tau}}{2} \end{pmatrix} \Psi_{\tau\mathbf{sk}}, \quad (1)$$

where $\Delta_{s\tau}$ is the spin and valley dependent gap, $v_F = ta$ is

the Fermi-velocity, a is the lattice constant, t is an effective hopping matrix element, and $\Psi_{\tau\mathbf{sk}}$ are two-component pseudospinors spanned by the d -type Mo-basis functions $|d_z^2\rangle$ and $(|d_{x^2-y^2}\rangle + i\tau|d_{xy}\rangle)/\sqrt{2}$. Eigenstates of H_0 have the relativistic dispersion $\epsilon_{s\tau k} = \sqrt{(\frac{\Delta_{s\tau}}{2})^2 + (\hbar v_F k)^2}$ and can be chosen such that they are simultaneous eigenstates of the operator $\hat{j}_z = \hat{L}_z + \frac{\tau}{2}\hat{\sigma}_z$:

$$\Psi_{s\tau\mathbf{k}}^j = \begin{pmatrix} \psi_A(k) e^{i(j-\tau/2)\theta_{\mathbf{k}}} \\ \psi_B(k) e^{i(j+\tau/2)\theta_{\mathbf{k}}} \end{pmatrix}. \quad (2)$$

Here, $\hat{L}_z = -i\hbar \frac{\partial}{\partial \theta_{\mathbf{k}}}$ and $\hat{\sigma}_z$ is the z -component of the pseudo-spin. Hence, the light-matter interaction is given by $H_I = -e \frac{v_F}{c} \sum_{s\tau\mathbf{k}} \Psi_{s\tau\mathbf{k}}^\dagger (A^{-\tau} \hat{\sigma}^+ + A^\tau \hat{\sigma}^-) \Psi_{s\tau\mathbf{k}}$ with $A^\tau = A_x + i\tau A_y$ and $\hat{\sigma}^\pm$ are the ladder operators. The optical selection rules are then given by $\langle \Psi_j | H_I | \Psi_{j'} \rangle \propto A^{-\tau} \delta_{j,j'+\tau} + A^\tau \delta_{j,j'-\tau}$, showing that excitation with right(left)-handed circular polarized light increases (decreases) the angular momentum \hat{j}_z by \hbar .

Since the MDF Hamiltonian in Eq. 1 does not display the full three-fold lattice rotational symmetry and does not account for the angular momentum change $-2\tau\hbar$ of the basis functions upon absorption, we propose to modify Eq. 1 by incorporating the three-fold rotational symmetry via

$$H_{\text{mMDF}} = \sum_{\tau\mathbf{sk}} \Psi_{\tau\mathbf{sk}}^\dagger \begin{pmatrix} \frac{\Delta_{s\tau}}{2} & \tau\hbar v_F k e^{-3i\tau\theta_{\mathbf{k}}} \\ \tau\hbar v_F k e^{3i\tau\theta_{\mathbf{k}}} & -\frac{\Delta_{s\tau}}{2} \end{pmatrix} \Psi_{\tau\mathbf{sk}}. \quad (3)$$

This modified massive Dirac Fermion (mMDF) Hamiltonian has the same relativistic dispersion as the original MDF Hamiltonian and the eigenstates have the general form

$$\tilde{\Psi}_{s\tau\mathbf{k}}^j = \begin{pmatrix} \psi_A(k) e^{i(j-3\tau/2)\theta_{\mathbf{k}}} \\ \psi_B(k) e^{i(j+3\tau/2)\theta_{\mathbf{k}}} \end{pmatrix}. \quad (4)$$

Using the minimal substitution, the light-matter interaction is obtained as

$$\tilde{H}_I = -e \frac{v_F}{c} \sum_{s\tau\mathbf{k}} \tilde{\Psi}_{s\tau\mathbf{k}}^\dagger \left(\frac{(A^{-\tau})^3}{A^2} \hat{\sigma}^+ + \frac{(A^\tau)^3}{A^2} \hat{\sigma}^- \right) \tilde{\Psi}_{s\tau\mathbf{k}}, \quad (5)$$

yielding the optical excitation rules $\langle \tilde{\Psi}_j | \tilde{H}_I | \tilde{\Psi}_{j'} \rangle \propto (A^{-\tau})^3/A^2 \delta_{j,j'+3\tau} + (A^\tau)^3/A^2 \delta_{j,j'-3\tau}$. Hence, excitation

with σ^\pm polarized light increases the angular momentum associated with the geometric phase by $\pm 3\hbar$, while simultaneously the angular momentum associated with the basis functions is decreased by $\pm 2\hbar$, in agreement with the conservation of the total angular momentum. Furthermore, for linearly polarized light, a rotation of the polarization angle by $2\pi/3$ does not alter the optical spectra, thus reflecting the three-fold lattice symmetry.

Although the eigenstates of our new mMDF Hamiltonian have the same unrenormalized dispersion as H_0 , the Coulomb matrix elements contain the electron-hole overlap matrix elements and hence differ in their geometric phases. In particular, the electron-hole Coulomb matrix element relevant for the description of the excitonic properties is given by

$$W_{\mathbf{k}-\mathbf{k}'}^{cvvc} = |u_{\mathbf{k}}u_{\mathbf{k}'} + v_{\mathbf{k}}v_{\mathbf{k}'}e^{-im(\theta_{\mathbf{k}}-\theta_{\mathbf{k}'})}|^2 W_{\mathbf{k}-\mathbf{k}'}.$$

Here, $W_{\mathbf{k}-\mathbf{k}'}$ is the screened quasi-two dimensional Coulomb potential and $u_{\mathbf{k}}^2 = (\epsilon + \frac{\Delta}{2})/2\epsilon$, $v_{\mathbf{k}}^2 = (\epsilon - \frac{\Delta}{2})/2\epsilon$, and $m = 1$ and $m=3$ for the MDF and mMDF Hamiltonian respectively. As a consequence, the Coulomb-renormalized band structure can be computed from the modified gap equations[22, 23]

$$\tilde{\Delta}_{\mathbf{k}} = \Delta + \frac{1}{2} \sum_{\mathbf{k}'} W_{|\mathbf{k}-\mathbf{k}'|} \frac{\tilde{\Delta}_{\mathbf{k}'}}{\mathcal{E}_{\mathbf{k}'}} \quad (6)$$

$$\tilde{v}_{\mathbf{k}} = v_F + \frac{1}{2} \sum_{\mathbf{k}'} W_{|\mathbf{k}-\mathbf{k}'|} \frac{k'}{k} \frac{\tilde{v}_{\mathbf{k}'}}{\mathcal{E}_{\mathbf{k}'}} \cos(m(\theta_{\mathbf{k}} - \theta_{\mathbf{k}'})), \quad (7)$$

$$\mathcal{E}_{\mathbf{k}} = \sqrt{\tilde{\Delta}_{\mathbf{k}}^2 + 4\hbar^2 \tilde{v}_{\mathbf{k}} k^2}, \quad (8)$$

with $m = 3$ instead of $m = 1$.

To calculate the renormalized dispersion from the gap equations, we computed the band structure and dipole-matrix elements via density functional theory (DFT) [24] utilizing the *Vienna ab initio simulation package* (VASP) [25–27] using the Perdew-Burke-Ernzerhof (PBE) functional [28], and including spin-orbit interaction[29]. Fitting the DFT band structure around the K points by the MDF dispersion, we obtain the MDF parameters for the gap and Fermi-velocity. The screened Coulomb potential within different dielectric environments is determined from Poisson's equation using the DFT screening parameters for the parent bulk material as described in Ref.[23], and the Coulomb matrix elements were calculated with the aid of the DFT wave-functions. Together with the gap equations, this provides a microscopically consistent description of the renormalized quasi-particle dispersion.

As shown in Ref.[23], within numerical accuracy the simultaneous solution of Eqs. 6, 7, and 8 with $m = 1$ leads to rigid band shifts without dispersion modifications. Interestingly, this aspect changes significantly once the renormalization of the Fermi-velocity properly includes the three-fold rotational symmetry. As an example, we compare in Fig. 1 the renormalized energy dispersion for a suspended monolayer of MoS₂ using the original MDF Hamiltonian (red dashed line) with that of the mMDF Hamiltonian (red solid line). The respective blue solid and dashed lines show the corresponding results for an hBN encapsulated monolayer.

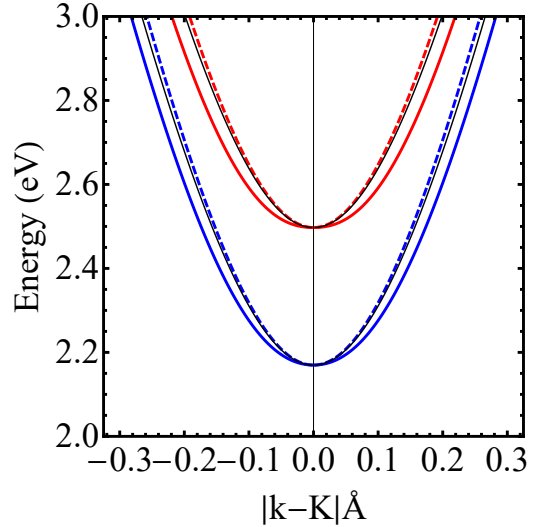


FIG. 1. Comparison of the renormalized dispersion at the K -valleys solving the gap equations with the mMDF Hamiltonian (solid lines) and the original MDF Hamiltonian (dashed lines) for the example of a suspended (red) and hBN encapsulated (blue) MoS₂ monolayer. The thin black lines show the unrenormalized dispersion shifted to match with the renormalized gap.

One clearly recognizes that the curvature of the mMDF dispersion at the bottom of the valleys is smaller as compared to the input DFT dispersion, i.e. the mMDF theory yields an enhanced effective mass, whereas the original MDF calculations merely yield a rigid shift of the unrenormalized dispersion. A quadratic fit in the region $|\mathbf{k} - \mathbf{K}| \leq 0.1 \text{ \AA}^{-1}$ yields

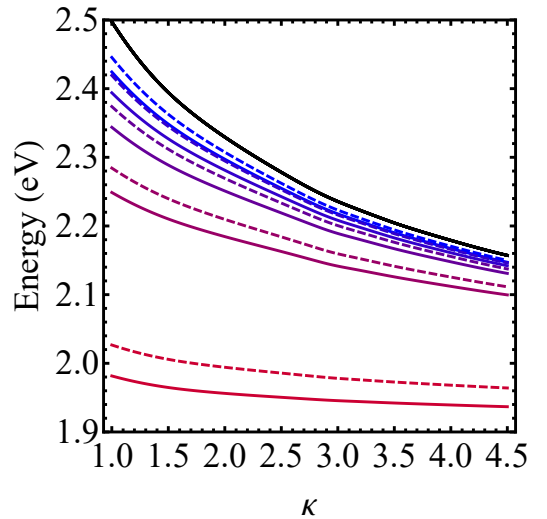


FIG. 2. Exciton resonance energies of MoS₂ as function of the dielectric environment represented by the effective dielectric constant $\kappa = (\epsilon_{\text{top}} + \epsilon_{\text{bottom}})/2$. The lowest five resonances (colored) and the band gap (black) are shown resulting from the modified mMDF Hamiltonian (solid lines) and the original MDF Hamiltonian (dashed lines).

the effective reduced masses of $m_r^{\text{vac}} = 0.4 m_0$ for the suspended monolayer in vacuum, and $m_r^{\text{hBN}} = 0.35 m_0$ for an hBN encapsulated MoS₂ monolayer ($m_r^{\text{vac}} = 0.326 m_0$ and $m_r^{\text{hBN}} = 0.312 m_0$ if fitted on $|\mathbf{k} - \mathbf{K}| \leq 0.2 \text{ \AA}^{-1}$). These values are in excellent agreement with the reported effective electron mass of $m_e \approx 2m_r = 0.7 m_0$ extracted from Shubnikovde Haas (SdH) oscillations in hBN encapsulated MoS₂ monolayers[30] and should be compared to the DFT value of the effective reduced mass $m_r^{\text{DFT}} = 0.261 m_0$. In the corresponding calculations for MoSe₂ (not shown here), we find the effective reduced masses $m_r^{\text{vac}} = 0.44 m_0$ and $m_r^{\text{hBN}} = 0.382 m_0$ for vacuum and hBN encapsulated, respectively, which is also in excellent agreement with the effective electron mass of $m_e = 0.8 m_0$ found for hBN encapsulated MoSe₂ extracted from experiments[31].

In Fig. 2, we plot the energies of the lowest exciton resonances computed with the mMDF Hamiltonian as function

$$\left(\mathcal{E}_\mathbf{k}^e[B] + \mathcal{E}_\mathbf{k}^h[B] + \frac{eB}{2m_r c} \hat{l}_z + \frac{e^2 B^2}{8m_r c^2} \hat{\mathbf{r}}^2 \right) \psi_\mu(\mathbf{k}) - \sum_{\mathbf{k}'} W_{|\mathbf{k}-\mathbf{k}'|}^{c\nu\nu c} \psi_\mu(\mathbf{k}') = E_\mu \psi_\mu(\mathbf{k}). \quad (9)$$

Here, m_r is the (unrenormalized) reduced mass of the electron-hole pair, \hat{l}_z is the angular momentum operator, $\hat{\mathbf{r}} = i\nabla_\mathbf{k}$ is the position operator, $W_{\mathbf{k}-\mathbf{k}'}^{c\nu\nu c}$ is the statically screened electron-hole Coulomb matrix element and $\mathcal{E}_\mathbf{k}^{e/h}[B]$ the renormalized single-particle dispersion that contains a Zeeman shift of the atomic orbitals contributing to the valence and conduction band. In general, the term $\propto \hat{l}_z$ leads to a Zeeman shift of the exciton states, however, for the s -type bright states this term does not contribute. The orbital angular momentum of d -type orbitals with $m_z = \pm 2$ leads to a Zeeman shift of $\pm 2\mu_B B$ of the valence band maxima, where $\mu_B = e\hbar/2m_0 c$ is the Bohr magneton, and a corresponding splitting between the K^\pm valleys. The Zeeman shift of the atomic orbitals enters the unrenormalized gap in Eq. 6 and is slightly enhanced by the gap-renormalization, leading to g -factors with an absolute value slightly larger than 4.

In the low magnetic field regime, the term $\propto B^2$ can be treated perturbatively, leading to a quadratic shift of the exciton resonance energy, which is the diamagnetic shift. In the high field limit and for a quadratic dispersion $\mathbf{p}^2/2m_r^*$, the term quadratic in B leads to the formation of Landau-levels with $E_n = \hbar\omega_c^*(n + 1/2)$, with a cyclotron frequency $\hbar\omega_c^* = \sqrt{m_r/m_r^*} \hbar\omega_c = e\hbar B/2\sqrt{m_r m_r^*} c$. Hence, in the high field limit the slope of the eigenvalues gives direct access to the mass renormalization, provided the dispersion is quadratic.

In Fig. 3, we compare the calculated diamagnetic shift $(E_{n,s}[B] + E_{n,s}[-B])/2$ using the mMDF dispersion for a freely suspended MoS₂ monolayer (dashed lines) with that of an hBN encapsulated configuration. The effective masses can be estimated from the slope at very high magnetic fields. A

of the dielectric environment represented by the effective dielectric constant $\kappa = (\epsilon_{\text{top}} + \epsilon_{\text{bottom}})/2$. The enhanced effective mass increases the exciton binding energy on a suspended monolayer from 471 to 560 meV, resulting in a resonance energy of 1.98 eV in vacuum. For the frequently used quartz substrate and hBN encapsulation, we use $\epsilon_{\text{top}} = 3.9$ and $\epsilon_{\text{top}} = \epsilon_{\text{bottom}} = 4.2$ and find the $1s$ -exciton resonances at 1.951 and 1.937 eV respectively.

To further investigate the consequences of the mass renormalizations predicted by the mMDF model, we compute the diamagnetic shift of the exciton resonances in TMDC systems. As has been suggested by Goryca et al.[32], the slope of the diamagnetic shift provides access to the effective exciton mass and, hence, can be used to test our theoretical predictions.

In a constant, perpendicular magnetic field, the exciton equation is given by[33]

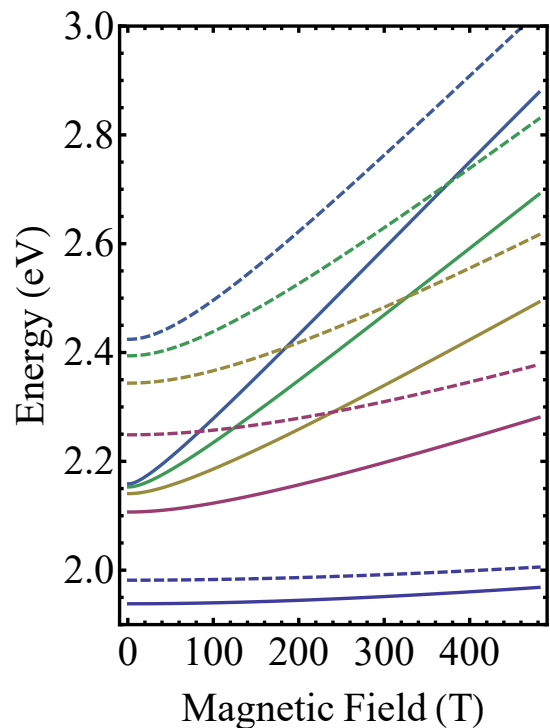


FIG. 3. Diamagnetic shift of the five lowest A-exciton states for a hBN encapsulated ML MoS₂ (solid lines) and a suspended MoS₂ ML (dashed lines) for magnetic fields up to 400 T. The effective exciton mass can be estimated from the slope of the diamagnetic shift at high fields.

linear fit in the region between 400 and 500 T yields a renor-

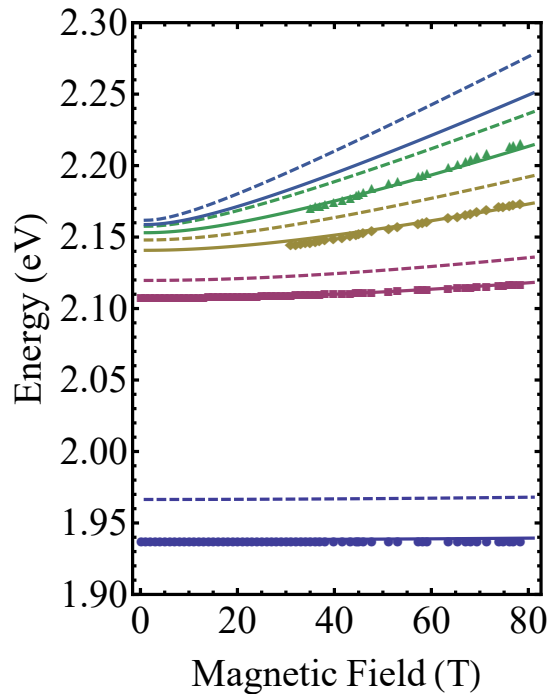


FIG. 4. Diamagnetic shift of the five lowest A-exciton states for a hBN encapsulated ML MoS₂ with threefold rotational symmetry (solid lines) and without threefold rotational symmetry (dashed lines). The enhanced exciton mass resulting from the three-fold rotational symmetry increases the exciton binding and reduces the slope at elevated magnetic fields. The discrete symbols denote experimental data points taken from reference 32.

malized exciton mass $m_r^{\text{hBN}} = 0.417 m_0$ for the hBN encapsulated sample, and $m_r^{\text{vac}} = 0.42 m_0$ for the suspended monolayer, respectively. These values are in reasonable agreement with those estimated from the dispersion.

To test the reliability of our calculations, we present in Fig. 4 a comparison of the mMDF calculated diamagnetic shift for the hBN encapsulated MoS₂ monolayer (solid lines) with experimental data taken from Ref. [32]. We obtain excellent agreement between theory and experiment which would not have been possible using the original MDF Hamiltonian (dashed lines). Equally good theory/experiment agreement has also been obtained for other TMDC systems, including MoTe₂, WS₂ and WSe₂. Data on these materials can be found in the supporting online material.

In conclusion, we introduced a modification of the original massive Dirac Fermion Hamiltonian that accounts for the three-fold rotational symmetry of the TMDC lattice. We show that this modified Hamiltonian leads to a curvature change in the computed energy band dispersion that depends on the dielectric environment. This renormalization of the effective mass manifests itself in the values of the predicted exciton binding energies and their magnetic field induced shift. We demonstrate excellent quantitative agreement with experimental data. Hence, we expect that the proposed modified massive Dirac Fermi Hamiltonian will find widespread use in future

experimental analysis and TMDC design applications.

ACKNOWLEDGEMENTS

This work was funded by the DFG via the Collaborative Research Center SFB 1083. We thank Scott Croocker for giving us access to their experimental data before publication.

- [1] D. Xiao, G.-B. Liu, W. Feng, X. Xu, and W. Yao, *Phys. Rev. Lett.* **108**, 196802 (2012).
- [2] A. Molina-Sánchez, D. Sangalli, K. Hummer, A. Marini, and L. Wirtz, *Phys. Rev. B* **88**, 045412 (2013).
- [3] T. Cao, G. Wang, W. Han, H. Ye, C. Zhu, J. Shi, Q. Niu, P. Tan, E. Wang, B. Liu, *et al.*, *Nature communications* **3**, 1 (2012).
- [4] H. Zeng, J. Dai, W. Yao, D. Xiao, and X. Cui, *Nature nanotechnology* **7**, 490 (2012).
- [5] K. F. Mak, K. He, J. Shan, and T. F. Heinz, *Nature nanotechnology* **7**, 494 (2012).
- [6] H. Zeng, G.-B. Liu, J. Dai, Y. Yan, B. Zhu, R. He, L. Xie, S. Xu, X. Chen, W. Yao, *et al.*, *Scientific reports* **3**, 1608 (2013).
- [7] Z. Li and J. P. Carbotte, *Phys. Rev. B* **88**, 045417 (2013).
- [8] S. Konabe and T. Yamamoto, *Phys. Rev. B* **90**, 075430 (2014).
- [9] C. Zhang, H. Wang, W. Chan, C. Manolatu, and F. Rana, *Phys. Rev. B* **89**, 205436 (2014).
- [10] T. C. Berkelbach, M. S. Hybertsen, and D. R. Reichman, *Phys. Rev. B* **92**, 085413 (2015).
- [11] H. Yu, M. Chen, and W. Yao, *National Science Review* **7**, 12 (2019), <https://academic.oup.com/nsr/article-pdf/7/1/12/32648413/nwz117.pdf>.
- [12] M. Tahir and U. Schwingenschlgl, *New Journal of Physics* **16**, 115003 (2014).
- [13] J. Li, L. Gu, and R. Wu, *Phys. Rev. B* **101**, 024412 (2020).
- [14] J. C. G. Henriques, G. Catarina, A. T. Costa, J. Fernández-Rossier, and N. M. R. Peres, *Phys. Rev. B* **101**, 045408 (2020).
- [15] N. D. Hien, C. V. Nguyen, N. N. Hieu, S. S. Kubakaddi, C. A. Duque, M. E. Mora-Ramos, L. Dinh, T. N. Bich, and H. V. Phuc, *Phys. Rev. B* **101**, 045424 (2020).
- [16] K. Zollner, P. E. Faria Junior, and J. Fabian, *Phys. Rev. B* **101**, 085112 (2020).
- [17] M. Shah and M. S. Anwar, *OSA Continuum* **3**, 878 (2020).
- [18] L. Chen, *Modern Physics Letters B* **0**, 2050181 (0), <https://doi.org/10.1142/S021798492050181X>.
- [19] H. Da, Q. Song, P. Dong, H. Ye, and X. Yan, *Journal of Applied Physics* **127**, 023903 (2020), <https://doi.org/10.1063/1.5118327>.
- [20] C. Bai and Y. Yang, *Journal of Physics: Condensed Matter* **32**, 085302 (2019).
- [21] H. M. Dong, Z. H. Tao, Y. F. Duan, F. Huang, and C. X. Zhao, *Journal of Physics: Condensed Matter* **32**, 125703 (2019).
- [22] T. Stroucken and S. W. Koch, in *Optical Properties of Graphene*, edited by R. Binder (World Scientific Publishing, Singapur, 2017) Chap. 2, pp. 43 – 84.
- [23] L. Meckbach, T. Stroucken, and S. W. Koch, *Phys. Rev. B* **97**, 035425 (2018).
- [24] W. Kohn and L. J. Sham, *Phys. Rev.* **140**, A1133 (1965).

- [25] G. Kresse and J. Hafner, Phys. Rev. B **47**, 558 (1993).
- [26] G. Kresse and J. Hafner, Phys. Rev. B **49**, 14251 (1994).
- [27] G. Kresse and J. Furthmüller, Comput. Mater. Sci. **6**, 15 (1996).
- [28] J. P. Perdew, K. Burke, and M. Ernzerhof, Phys. Rev. Lett. **77**, 3865 (1996).
- [29] S. Steiner, S. Khmelevskiy, M. Marsmann, and G. Kresse, Phys. Rev. B **93**, 224425 (2016).
- [30] R. Pisoni, A. Kormányos, M. Brooks, Z. Lei, P. Back, M. Eich, H. Overweg, Y. Lee, P. Rickhaus, K. Watanabe, T. Taniguchi, A. Imamoglu, G. Burkard, T. Ihn, and K. Ensslin, Phys. Rev. Lett. **121**, 247701 (2018).
- [31] S. Larentis, H. C. P. Movva, B. Fallahazad, K. Kim, A. Behroozi, T. Taniguchi, K. Watanabe, S. K. Banerjee, and E. Tutuc, Phys. Rev. B **97**, 201407 (2018).
- [32] M. Goryca, J. Li, A. V. Stier, T. Taniguchi, K. Watanabe, E. Courtade, S. Shree, C. Robert, B. Urbaszek, X. Marie, *et al.*, Nature communications **10**, 1 (2019).
- [33] A. V. Stier, N. P. Wilson, K. A. Velizhanin, J. Kono, X. Xu, and S. A. Crooker, Phys. Rev. Lett. **120**, 057405 (2018).